Dynamics of Transversal Hot Zones in Shallow Packed-Bed Reactors†

Bharat Marwaha, Sandhya Sundarram, and Dan Luss*

Department of Chemical Engineering, University of Houston, Houston, Texas 77204-4792

Received: January 14, 2004; In Final Form: April 7, 2004

Infrared thermography was used to study the evolution and dynamics of hot zones on the top of a shallow packed-bed reactor (10 cm in diameter), packed with spherical catalyst pellets (Pd/Al_2O_3). The test reaction, the atmospheric oxidation of carbon monoxide, was run under conditions for which steady-state multiplicity exists. Slow cooling of the vessel housing the reactor close to its extinction temperature shifted the reactor from a fully ignited state to one with a hot region, separated by a sharp temperature front from the adjacent colder region ($\Delta T = 75$ °C for a feed of 6 vol % CO). The hot zone exhibited one of three qualitatively different motions: a breathing motion, an antiphase (standing wave) motion, or a hopping motion. In breathing motion, a the sharp temperature front moved back-and-forth. The breathing frequency increased upon cooling of the reactor. In antiphase motion, the hot zone moved rapidly and periodically from one side of the reactor to the other. In hopping motion, the hot zone rotated around the reactor, followed by a periodic rest at some locations. The angular velocity of the rotating hot zone and its size changed with angular position. Slow cooling of the reactor led to the following sequence of bifurcations (breathing → antiphase → hopping) Preliminary experiments suggest that global coupling between the top of the bed and the unconverted reactants stabilized the spatiotemporal patterns, which may not exist in its absence.

1. Introduction

The transversal (normal to the flow direction) temperature in an adiabatic reactor is usually uniform. However, transversal hot zones are known to exist in adiabatic packed-bed reactors. For example, Boreskov et al.[1] observed several hot regions in the bottom of a packed-bed reactor during the partial oxidation of isobutyl alcohol. Barkelew and Gambhir[2] reported that small agglomerates of molten catalytic pellets (clinkers) formed in a trickle-bed reactor during the hydrodesulfurization of crude oil. Moving hot zones were observed in Pt−Rh gauze convertors used in the synthesis of HCN and ammonia oxidation. Nonuniform activity or packing in the reactor can generate transversal hot zones. It may also be induced by natural convection at low velocity of the reacting mixture.[3,4] However, at present it is not known what causes the formation of transversal hot zones in a uniformly active packed-bed reactor under the common situation that forced convection dominates the reactants' transport. Balakotaiah et al.[5] showed that hot zones may form when the characteristic time of transversal reactant dispersion is shorter than that of the temperature dispersion. However, Yakhanin and Menzinger[6] pointed out that in practice the heat dispersion largely exceeds that of the species. Nekhamkina et al.[7] observed a contracting and expanding transverse hot zone on a glass-fiber catalytic cloth during CO oxidation.

The formation of hot zones may have a deleterious impact on the yield of the desired product(s) and may deactivate the catalyst. Moreover, a hot zone existing next to the reactor walls may cause severe safety problems by decreasing the wall's mechanical strength. This may generate a leak that may lead to an explosion. Understanding and being able to predict the formation of these hot zones is of both practical importance and intrinsic academic interest. This information is essential for developing operation and control procedures that avoid the formation of these hot spots, or at least for minimizing their magnitude. To accomplish this goal we have started an investigation of the formation and dynamics of transverse temperature patterns in shallow packed-bed reactor during the atmospheric oxidation of carbon monoxide.[8−10] The results reported here are part of that study.

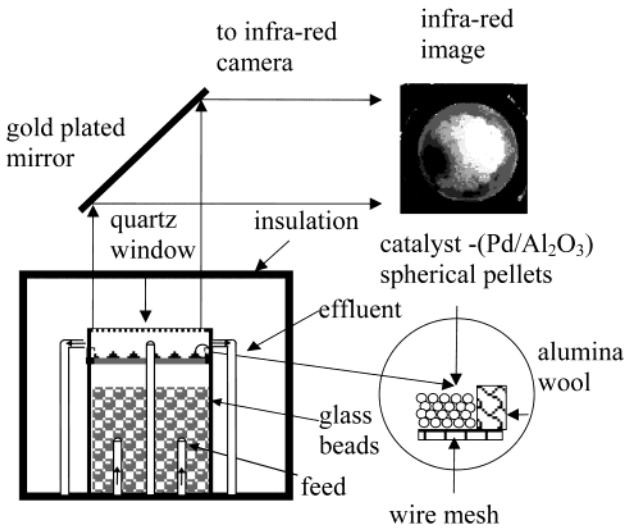

Figure 1. Schematic of the experimental system used to investigate the formation and dynamics of hot zones.

2. Experimental Setup and Procedure

Infrared imaging was used to follow the formation and motion of transverse hot zones in a shallow packed-bed reactor during the atmospheric oxidation of carbon monoxide. The reactor was a cylindrical stainless steel (SS 316) vessel (125 mm o.d., 5 mm wall thickness, 286 mm long). The shallow packed bed

† Part of the special issue "Gerhard Ertl Festschrift".

* Corresponding author. E-mail: dluss@uh.edu.

10.1021/jp049803p CCC: $27.50
Published on Web 06/22/2004

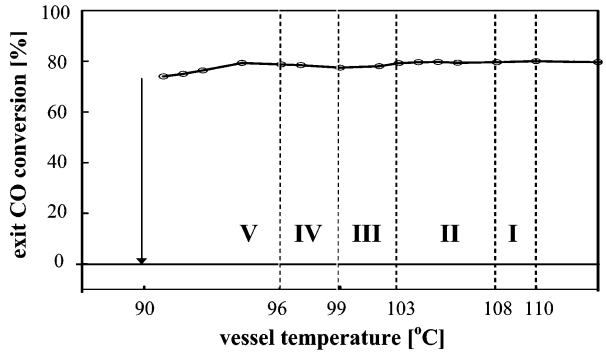

Figure 2. Bifurcation diagram showing five different regions denoting sequence of evolution of noninform states (I, breathing motion; II, antiphase motion; III, rotation/hopping motion; IV, hopping motion with one step; and V, hopping motion with two steps) upon cooling the vessel.

consisted of several layers of 2−3 mm diameter spherical catalyst pellets (0.5 wt % palladium deposited in a thin exterior shell on alumina). The catalyst pellets were uniformly packed on top of a thin stainless steel wire mesh, supported on three stainless steel pins, 51 mm from the top of the vessel. Preliminary experiments have shown that conductive heat loss due to contact between the vessel wall and catalyst affects the temperature profile and causes premature extinction. To minimize this heat loss, alumina wool was packed in an annular space (3 mm) between the catalyst pellets and the vessel wall (Figure 1). The cylindrical vessel housing the packed bed was thermally insulated and electrically heated from the outside. The vessel wall temperature was measured by thermocouples and regulated by a temperature controller (PID, Omega CN2041). The effluent (CO) concentration was measured by an infrared gas analyzer (AR-411; Anarad), at a sampling frequency of 0.1 Hz.

The reactive mixture was fed into the reactor through five 6-mm inlet ports at the vessel bottom (four on the periphery and one in the center) and exited through four 6-mm outlet ports at the top. To enhance the feed distribution, the bottom of the vessel was packed with glass beads to a height of 127 mm. The reactive feed consisted of extra-dry-grade oxygen (purity 99.6%), carbon monoxide (Aramax), and purified-grade nitrogen (purity 99.998%). The carbon monoxide was purified by passing through a molecular sieve adsorbent (5A zeolite; Linde) carbonyl trap. The feed gases were mixed in a bed of glass beads, purified, and dried by activated charcoal purifiers (Linde) before entering the vessel. The gas flow rates were regulated by thermal mass flow controllers (FC-280, FC-261, and FC-260; Tylan; accuracy ±1%). In all the experiments reported here, the feed contained 6 vol % CO, 70 vol % O_2, and 24 vol % N_2. The total flow rate was 1600 cm^3/min unless specified otherwise.

The top cover of the SS 316 vessel was an infrared-transparent quartz disk. The temperature distribution, on the top layer of catalyst pellets, was monitored by an IR camera (Amber Radiance PM). A gold-plated mirror, inclined by 45° above the vessel, reflected the radiation from this layer to the infrared camera. It had a 256 × 256 indium−antimonide detector array, sensitive to 3−5 μm radiation. The field of view of its 50 mm lens was 11° × 11° and the spatial resolution was 0.4 mm^2.

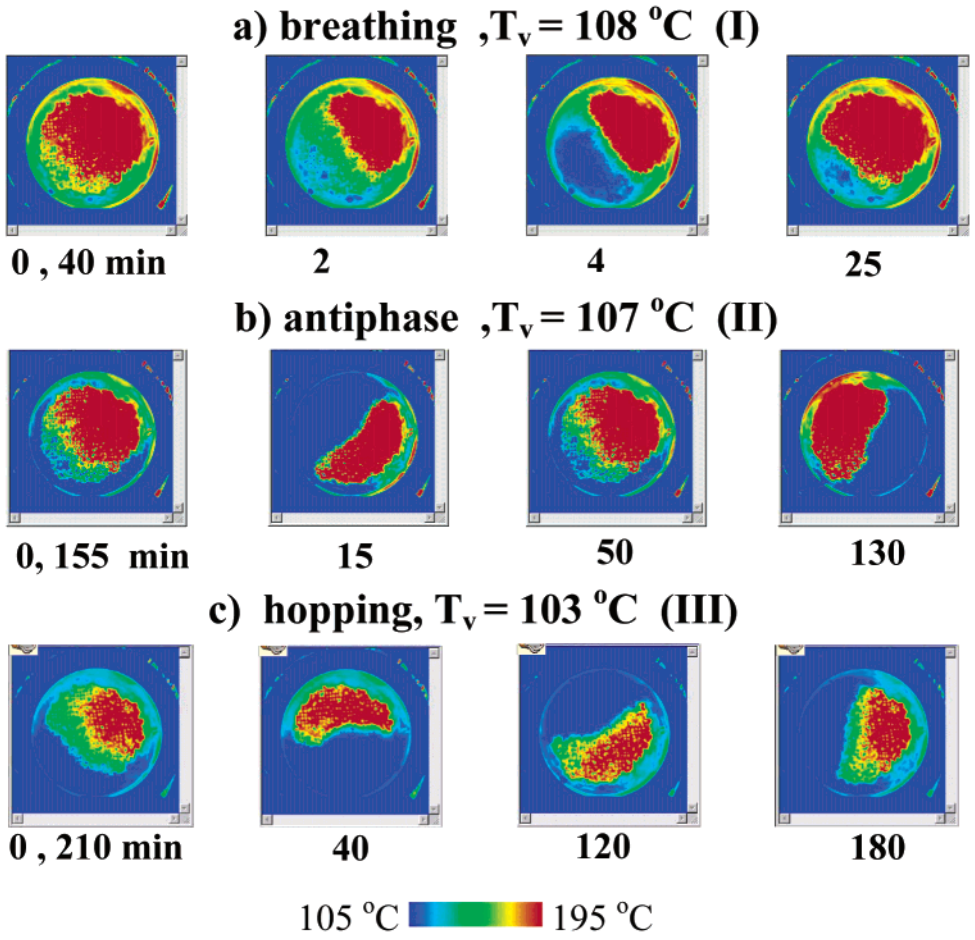

Figure 3. Snapshots of temperature distribution on the top surface of the bed for a hot zone exhibiting breathing motion (a), antiphase motion (b), and modulated rotation/hopping motion (c).

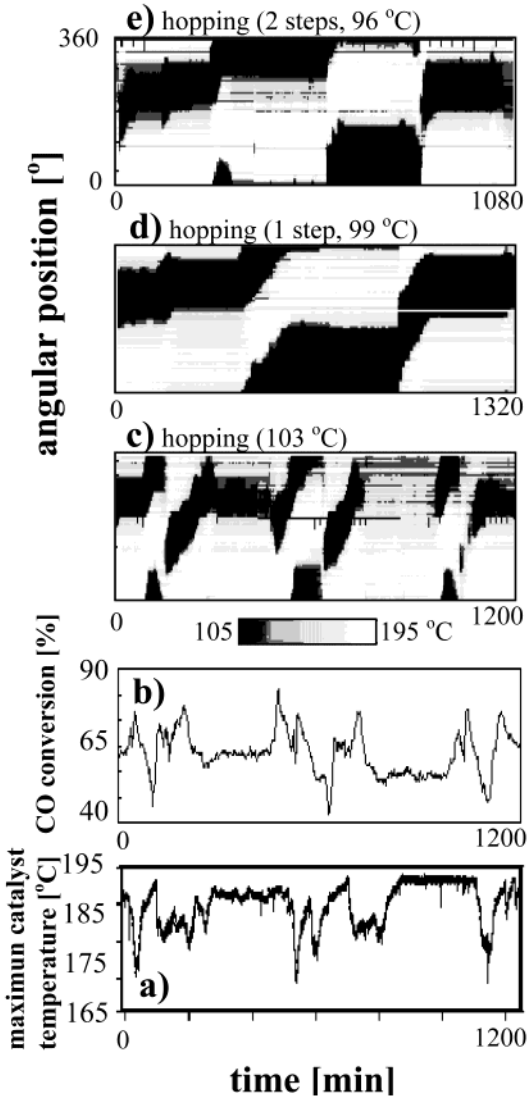

Figure 4. (a) Fluctuation in the maximum catalyst temperature and (b) exit CO conversion during three rotation cycles of the hot zone at vessel temperature of 103 °C. (c) The corresponding temporal angular position (on a concentric circle with $R = 0.8R_o$) vs time plot. At vessel temperatures of 99 °C (d) and 96 °C (e), the hot zone becomes stationary during each rotation at two and three locations, respectively.

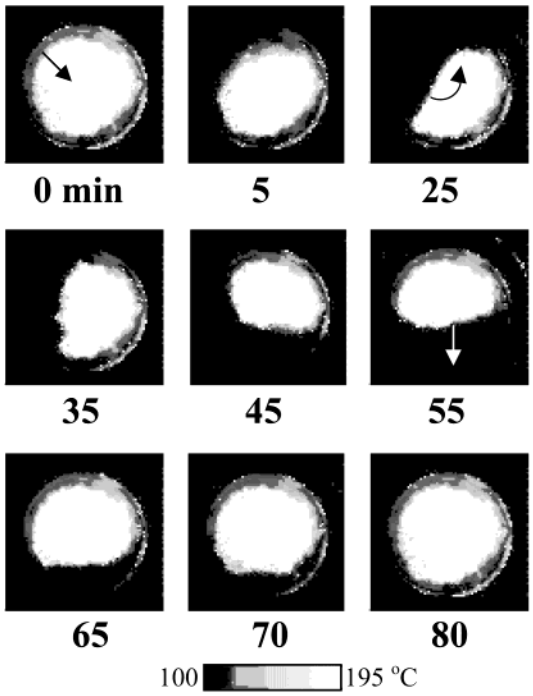

Figure 5. A mixed mode motion of both breathing and rotation of the hot zone at a vessel temperature of 95 °C and total flow rate of 2400 cm^3/min. The arrows indicate the direction of front motion.

The measured temperatures were recorded on a computer using Imagedesk II software (Raytheon Amber).

The vessel temperature was stepwise increased during an experiment from room temperature until the whole packed bed (top surface) was ignited and attained a uniform, high temperature. After attaining a fully ignited state, the vessel temperature was stepwise decreased until the reactor extinguished. We waited at each vessel temperature till a stationary state was reached (1.5−2 h) before recording any infrared images. A typical run took 36 h, with 75 % of the data taken close to the extinction point, as patterned states were found only in that region. IR images were recorded at the rate of one to four images per minute to effectively capture the slow hot zone motion.

3. Experimental Results

Nonuniform states evolved from a fully ignited state in a reactor, packed with a single layer of catalyst pellets, following a stepwise decrease in the vessel temperature. Increasing the vessel temperature led to ignition at 160 °C. The temperature at the top of the bed of this ignited state (conversion ≅ 80%) was high and uniform. As the vessel was slowly cooled from 160 °C, the hot region covering the entire catalyst surface initially cooled uniformly. However, at 110 °C, the temperature on the top surface became nonuniform and a cold region formed in the periphery of the bed. A sharp temperature front ($\Delta T = 75$ °C) separated the regions of high and low temperatures. The bifurcation diagram (Figure 2) shows the dependence of the time-averaged effluent CO conversion on the bifurcation parameter, the vessel temperature. Spatiotemporal temperature patterns formed on the top of the catalyst bed as the reactor was cooled below 110 °C. These temperature patterns were accompanied by oscillations in the effluent CO conversion. The front motion became more complex as the vessel temperature decreased. Extinction of the high-temperature state occurred at 90 °C.

The cooling led to formation of three qualitatively different spatiotemporal patterns (nonuniform states). Figure 2 shows the range of vessel temperature in which these motions occurred, and Figure 3 shows snapshots of the states in regions I, II, and III of Figure 2. In region I (vessel temperatures between 108 and 110 °C), the temperature front moved back-and-forth, causing contraction and expansion of hot region. We define this motion as *breathing.* Figure 3a shows snapshots of the temperature on the top of the packed bed during one breathing cycle at a vessel temperature of 108 °C (region I). The hot zone (Figure 3a) shrank for about 4 min and then slowly expanded, returning to the original size after 40 min. The average front velocity during the contraction (2.5 cm/min) was much faster than that during the subsequent expansion (0.1 cm/min).

Standing temperature waves (antiphase oscillations) with some breathing imposed on it existed in region II. During this periodic motion the hot region oscillated between two diametrically opposite mirror image locations, shown by the snapshots at 15 and 130 min (Figure 3b). It took 115 min for the transition from the state attained at 15 min to that at 130 min. However, the reverse transition took only 40 min. Moreover, many of the intermediate states are not symmetric

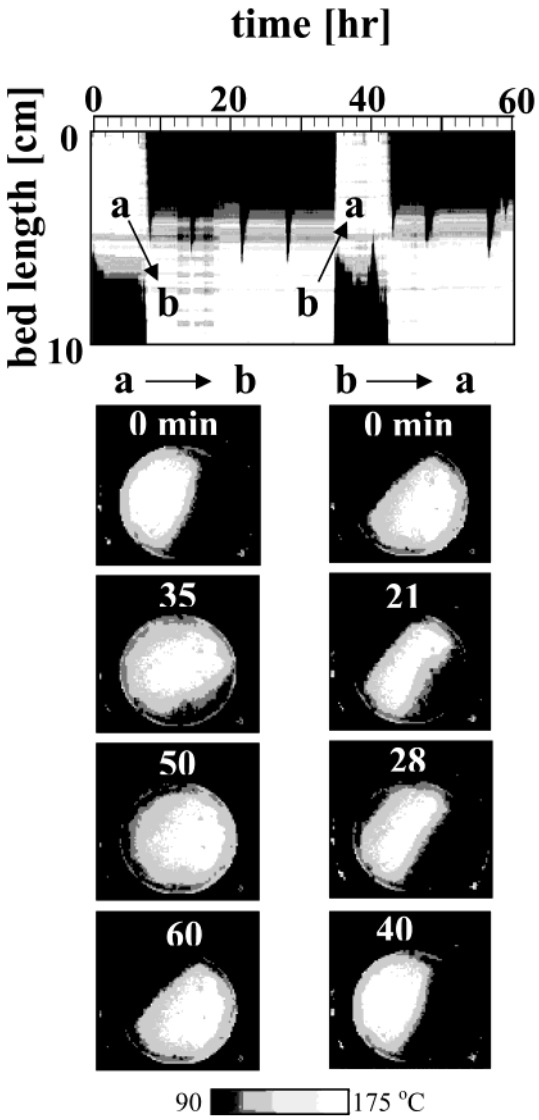

Figure 6. Complex transverse motion exhibited by a hot zone on the top of a bed packed with two layers of catalyst. The motion of the hot zone from a to b differs from its return from b to a.

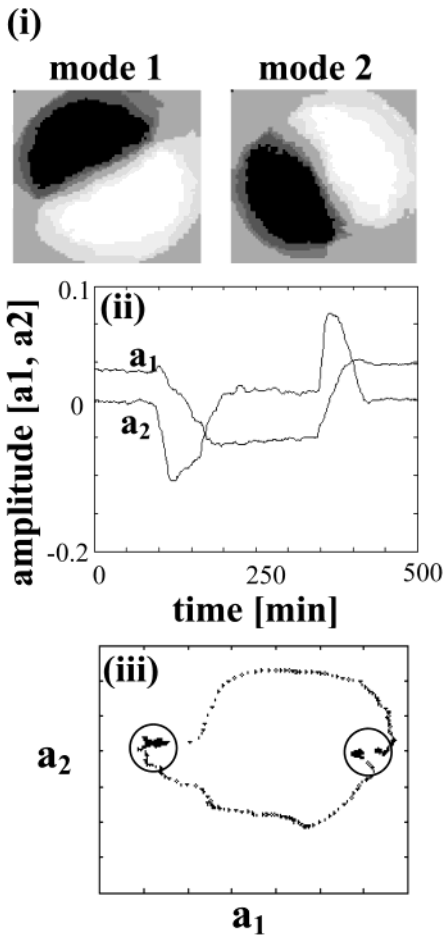

Figure 7. POD of a hopping motion when the hot zone remained stationary for a long time at two locations (Figure 4). (i) The first two modes, (ii) the temporal amplitudes of the two modes, and (iii) their phase portrait. The circles in part iii indicate the two location where the hot zone halted for a long time.

with respect to a rotation by π. This antiphase motion deviates from that of a classical standing wave.

In region III (vessel temperature between 103 and 99 °C), the hot region rotated on the top of the bed at a nonconstant angular velocity and its size changed during the rotation (40 and 180 min, Figure 3c). After completing one rotation, the hot region became stationary for awhile before the start of a new rotation. Whenever the hot zone contracted, the exit CO conversion decreased (Figure 4b) while the maximum catalyst temperature increased (Figure 4a) and vice versa. A space−time plot (Figure 4c) of the temporal angular temperature at a fixed radial position shows that a complete rotation of the hot zone took about 3.5 h. The hot zone then remained stationary for 4−5 h before starting another rotation. The space−time plot (Figure 4c) shows that a small breathing motion was superimposed on this modulated hopping motion.

As the vessel temperature was further decreased, the rotating pulse became stationary for awhile twice (region IV, $97 \leq T \leq 99$) or three times (region V, $91 \leq T \leq 96$) during each rotation. Angular position−time plots of these motions are shown in Figure 4d,e. Antiphase oscillations were not observed in region IV and V. The same sequence of bifurcation of the nonuniform states (breathing → antiphase → hopping) was observed at various flow rates and for a different number of catalyst layers in the bed.

As the breathing persisted till extinction, the reactor sometimes reached a nonuniform state that combined the breathing and hopping (rotation) modes. Figure 5 illustrates such a complex mixed mode pattern obtained at a vessel temperature of 95 °C and a total flow rate of 2400 cm^3/min. During the first 25 min, an extinction wave caused shrinking of the hot zone. The direction of the extinction wave is marked by an arrow in the snapshot at 0 min (Figure 5). Then the rotation mode became more dominant than breathing, and the hot zone rotated in the counterclockwise direction for 30 min. Then at 55 min, breathing became again dominant, and the hot zone expanded to its original size, as indicated by an arrow at that snapshot.

A complex motion of the hot zone was observed in a bed packed with two layers of catalyst pellets at a vessel temperature of 87 °C. During this motion, which had a rather long period of 10−20 h, the hot zone alternated between two diametrically opposite locations (a and b, in Figure 6) by a traveling across the surface of the bed. The two columns of snapshots a → b and b → a in Figure 6 show the difference in the two transitions between the two locations. During the motion from a to b, the hot zone expanded for 35 min and occupied almost the whole surface. The hot zone then shrank and occupied only region b. The hot zone moved in the form of a band across the bed from position b to a. The evolution of the temperature along a line (of length 10 cm), aligned in the direction of a and b, during

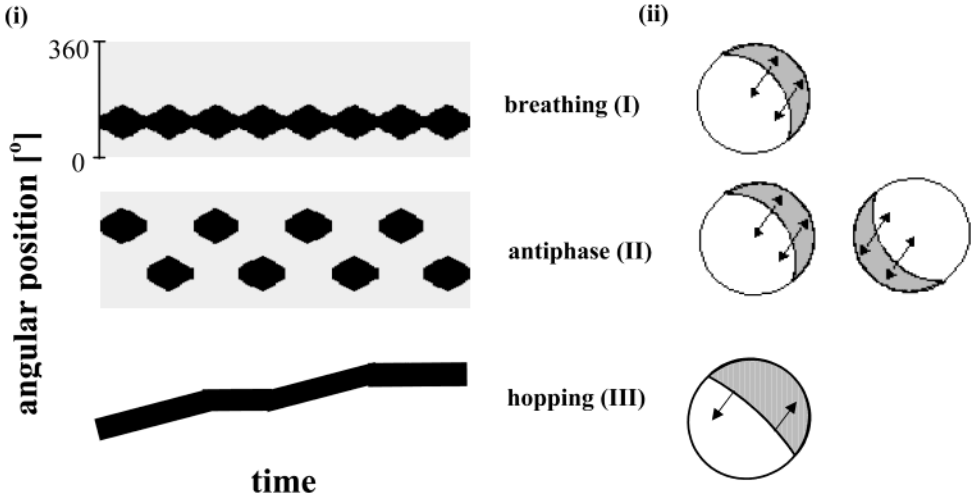

Figure 8. (i) Schematic of space−time and (ii) snapshots of the catalyst bed under breathing, antiphase, and hopping motion.

this complex motion is shown in Figure 6. The space−time plot also shows that the hot zone undergoes breathing during its rather long stay at locations a and b.

4. Discussion

It is well-established that the activity of commercial catalysts is usually nonuniform. Pawlicke and Schmitz[11] found in their pioneering IR thermography experiments that the activity of commercial catalytic pellets is nonuniform. Graham et al.[12] and Somani et al.[13] observed that the speed, size, and direction of rotating pulses during the oxidation of hydrogen on a thin nickel ring depended on the azimuthal position due to catalyst nonuniformities. Otterstedt et al.,[14] reported that a nonuniform surface created a similar azimuthally dependent rotating pulse motion in electrochemical systems. Christoph et al.[15] and Grauel et al.[16] observed modulated rotating pulses during electrochemical action on a ring electrode, similar to the modulated hopping motion observed by us (Figure 4c).

The initial nonuniformity of the catalytic surfaces becomes even larger after being used to carry out exothermic reactions. Moreover, the local transport coefficients on the surface of a catalytic pellet are usually nonuniform. These nonuniformities distorted the features of the patterns we observed from those obtained on a uniformly active media. The nonuniformity is most probably the cause of the nonideal standing wave shown in Figure 3b, as well the dependence of the local velocity and shape of the rotating temperature pulse on the azimuthal position and the hopping motion shown in Figure 4c−e. To determine the main dynamic features of the hopping motion, we conducted a proper orthogonal decomposition (POD)[17,18] analysis of the spatiotemporal images. Figure 7i shows the first two modes of the hopping motion shown in Figure 4d. These two modes account for over 90% of the total energy and are out-of-phase by 90°. Their periodic temporal amplitudes (a_1 and a_2) are symmetric about the time axis. The phase plane of the two amplitudes (Figure 7iii) is a closed curve, containing two dense regions, indicated by circles in phase space. These two locations represent the almost constant amplitudes obtained during the long sojourn of the hot zone at one of two locations, shown in Figure 4d.

Three qualitatively different motions existed in our experiments, breathing, antiphase, and hopping, shown schematically in Figure 8. A decrease in the temperature led to the following sequence of bifurcations (breathing → antiphase → hopping). Schematic snapshots of the catalyst bed in Figure 8ii show that the front initially moved as a single entity during the breathing and antiphase motion. However, following additional cooling, one part of the front moved in one direction, while the second moved in the opposite direction. This led to a rotation, and the nonuniformity caused the hot zone to become stationary at some less active locations, generating the complex hopping motion.

Horvath et al.[19] and Hagberg and Meron[20] have shown that a stationary front can be destabilized by an increase in the ratio of the time constant of the inhibitor to that of the autocatalytic variable in a two-variable diffusion-reaction system. This scenario may explain the sequence of bifurcations that we observed. The limiting reactant concentration is the inhibitor in our system, and its time constant ($1/k$, the pseudo-first-order reaction rate constant) is a strong, decreasing function of the temperature. The time constant of the autocatalytic variable, the temperature, depends on the transport coefficients and physical properties and is rather insensitive to temperature changes. Thus, decreasing the vessel temperature increased the ratio of the time constant of the inhibitor to that of the autocatalytic variable. This, in turn, destabilized the temperature front and increased the complexity its motion.

Analysis of the experimental data revealed that under the same operating conditions, the hot zone could travel by different motions/paths between two locations, at which it rested for some time. Such a motion is shown in Figure 6. The schematic Figure 9i illustrates three basic heteroclinic paths (counterclockwise rotation, clockwise rotation, and antiphase motion) that may be taken by a hot zone traveling between the two unstable locations x and y. For example, the hot zone at x can travel to y either via path xay (counterclockwise rotation), xby (clockwise rotation), or xcy (antiphase motion). Snapshots of three such motions are shown Figure 9ii. The same scenario was used by Graham et al.[21] to explain the motion of a temperature pulse on a nickel ring, catalyzing the oxidation of hydrogen.

The three qualitatively different spatiotemporal patterns (breathing, antiphase, and hopping) and the sequence of bifurcations between them we observed is strikingly similar to the 2D spatiotemporal patterns observed/simulated in electrochemical systems.[22−25] Birzu et al.[23] concluded that (negative) global coupling was the cause of the spatiotemporal patterns that they observed during the electrodissolution of a metal disk electrode. Similarly, Lee et al.[25] showed that these patterns may be generated by adjusting the magnitude of the nonlocal coupling during electro-oxidation of formic acid on a platinum ring electrode. The sequence of pattern bifurcations they

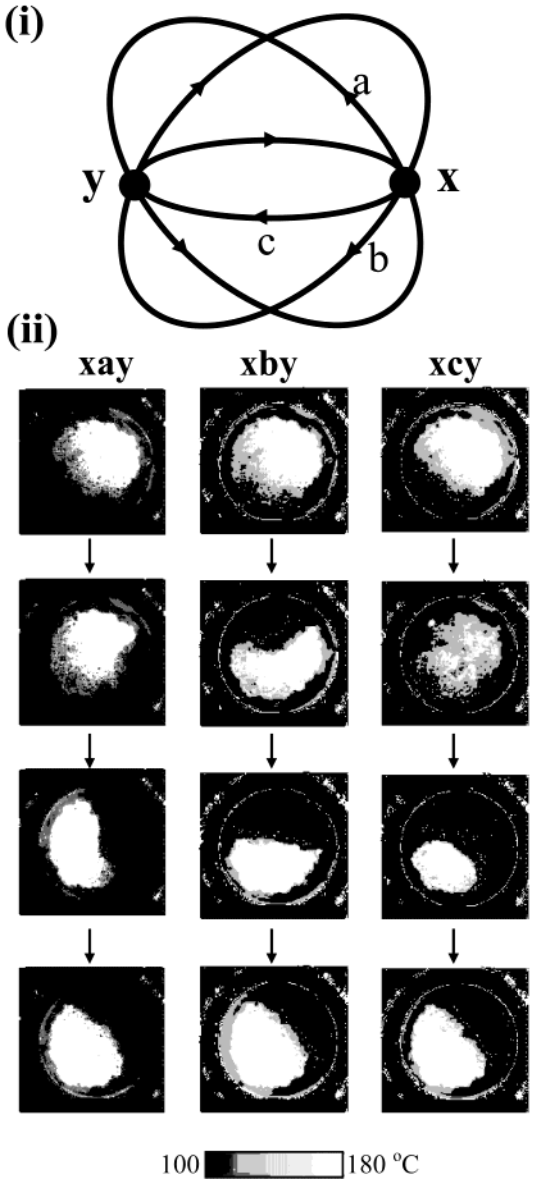

Figure 9. (i) Schematic of the three heteroclinic paths taken by hot zone to travel from location *x* to *y*. (ii) Experimentally observed hot zone motions.

observed under sufficient strength of the negative nonlocal coupling was similar to the sequence of breathing → antiphase → hopping that we observed. The formation of spatiotemporal temperature patterns on catalytic wires and ribbons due to global coupling (via electric control of temperature) was reported by Volodin et al.[26] and Lobban et al.[27] The impact of global coupling on the formation of spatiotemporal temperature patterns on catalytic surfaces was analyzed by Middya et al.[28] Such patterns were later observed on several catalytic systems, such as a ring,[29,30] hollow cylindrical pellet,[31] and a radial-flow packed-bed reactor.[8] Global coupling in our system may be caused by the contact between the unconverted reactants in the top of the reactor and the top of the catalyst pellets. This global coupling can stabilize the temperature front around the hot zone. This possible presence of global coupling is supported by Figure 10, which shows that extinction of the hot zone in one location (0 and 1 min) led to ignition at a different location (2 and 5 min). The increase in the reactant concentration at the top of the bed upon the extinction probably was the cause of the ignition at the other location. We are currently studying the affect of global coupling by changing the residence time of the gas at the top of the reactor.

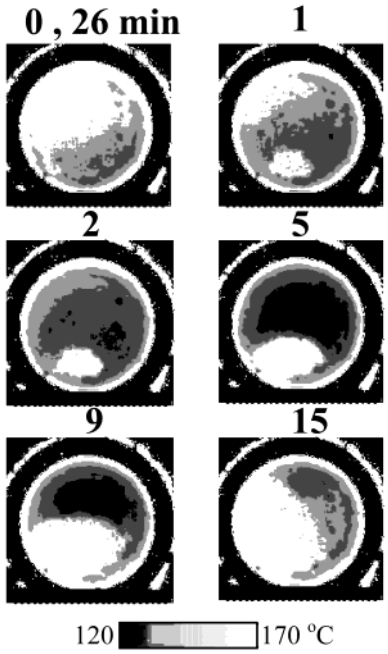

Figure 10. The extinction of a hot zone and a simultaneous ignition at another location (1 min) at a vessel temperature of 115 °C suggests the presence of global coupling.

Hartmann et al.[32] investigated chemical pattern formation on a microstructured Pt(100) surface during NO + CO reaction. They observed that rotating pulses existed in small circular domains and spiral waves in larger domains. This suggests that spiral waves are more likely to exist in large diameter, industrial reactor than in small diameter, laboratory, packed-bed reactors.

Acknowledgment. The authors wish to acknowledge the support of this research by grants from the National Science Foundation and the Welch Foundation.

References and Notes

(1) Boreskov, G. K.; Matros, Yu. Sh.; Klenov, O. P.; Lugovskoi, V. I.; Lakhmostov, V. S. *Dokl. Akad. Nauk SSSR* **1981**, *258*, 1418.
(2) Barkelew, C. H.; Gambhir, B. S. *ACS Symp. Ser.* **1984**, *237*, 61.
(3) Nguyen, D.; Balakotaiah, V. *Chem. Eng. Sci.* **1994**, *49*, 5489.
(4) Benneker, A. H.; Kronberg, A. E.; Westerterp, K. R. *AIChE J.* **1998**, *44*, 263.
(5) Balakotaiah, V.; Christoforatou, E. L.; West, D. H. *Chem. Eng. Sci.* **1999**, *54*, 1725.
(6) Yakhnin, V.; Menzinger, M. *Chem. Eng. Sci*. **2001**, *56*, 2233.
(7) Nekhamkina, O.; Digilov, R.; Sheintuch, M. *J. Chem. Phys.* **2003**, *119*, 2322.
(8) Marwaha, B.; Annamalai, J.; Luss, D. *Chem. Eng. Sci.* **2001**, *56*, 89.
(9) Marwaha, B.; Luss, D. *AIChE J.* **2002**, *48*, 617.
(10) Marwaha, B.; Luss, D. *Chem. Eng. Sci*. **2003**, *58*, 733.
(11) Pawlicke, P. C.; Schmitz, R. A. *Chem. Eng. Prog.* **1987**, *83*, 40.
(12) Graham, M. D.; Lane, S. L.; Luss, D. *J. Phys. Chem.* **1993**, *97*, 889.
(13) Somani, M.; Liauw, M. A.; Luss, D. *Chem. Eng. Sci.* **1997**, *52*, 2331.
(14) Otterstedt, R. D.; Plath, Jaeger, N. I.; Hudson, J. L. *Phys. Rev. E.* **1996**, *54*, 3744.
(15) **)** Christoph, J.; Otterstedt, R. D.; Eiswirth, M.; Jaeger, N. I.; Hudson, J. L. *J. Chem. Phys.* **1999**, *110*, 8614.
(16) Grauel, P.; Varela, H.; Krischer, K. *Faraday Discuss.* **2001**, *120*, 165.
(17) Fukunaga, K. In *Introduction to Statistical Pattern Recognition*; Academic Press: Boston, 1990.
(18) Graham, M. D.; Lane, S. L.; Luss, D. *J. Phys. Chem*. **1993**, *97*, 889.

(19) Horvatth, D.; Petrov, V.; Scott, S. K.; Showlater, K. *J. Chem. Phys*. **1993**, *98*, 6332.
(20) Hagberg, A.; Meron, E. *Nonlinearity* **1994**, *7*, 805.
(21) Graham, M. D.; Lane, S. L.; Luss, D. *J. Phys. Chem*. **1993**, *97*, 7564.
(22) Hudson, J. L.; Tabora, J.; Krischer, K.; Kevrekidis, I. G. *Phys. Lett. A* **1993**, *179*, 355.
(23) Birzu, A.; Plenge, F.; Jaeger, N. I.; Hudson, J. L.; Krischer, K. *J. Phys. Chem. B* **2003**, *107*, 5825.
(24) Plenge, P.; Rodin, P.; Schöll, E.; Krischer, K. *Phys. Rev. E* **2001**, *64*, 056229.
(25) Lee, J.; Christoph, J.; Strasser, P.; Eiswirth; Ertl, G. *Phys. Chem. Chem. Phys*. **2003**, *5*, 935.
(26) Volodin, Y. E.; Barelko, V. V.; Merzhanov, A. G. *Sov. J. Chem. Phys.* **1982**, *5*, 1142.
(27) Lobban, L.; G. Philippou, G.; Luss, D. *J. Phys. Chem.* **1989**, *93*, 733.
(28) Middya, U.; Luss, D.; Sheintuch, M. *J. Chem. Phys*. **1994**, *100*, 3568.
(29) Lane, S. L.; Luss, D. *Phys. Rev. Lett.* **1993**, *70*, 830.
(30) Annamlai, J.; Ballandis, C.; Somani, M.; Liauw, M. A.; Luss, D. *J. Chem. Phys*. **1997**, *107*, 1896.
(31) Annamalai, J.; Liauw, M. A.; Luss, D. *Chaos* **1999**, *9*, 36.
(32) Hartmann, N.; Bar, M.; Kevrekidis, I. G.; Krischer, K.; Imbihl, R. *Phys. Rev. Lett*. **1996**, *76*, 1384.